Nuclear Instruments and Methods in Physics Research A329 (1993) 348-360
North-Holland

NUCLEAR
INSTRUMENTS
& METHODS
IN PHYSICS
RESEARCH
Section A

An rf-linac, FEL buncher

W.A. Barletta [a], G. Bellomo [b], R. Bonifacio [b], R. Corsini [b], L. De Salvo [b], P. Pierini [b] and M. Pullia [b]

Lawrence Livermore National Laboratory, Livermore, CA, 94550, USA,
and Department of physics, University of California Los Angeles, 405 Hilgard Avenue, Los Angeles, CA, USA
n INFN and Universaà degh Studi, Via Celoria, 16, 20133 Milano, Italy

Received 2 December 1992

We describe a means of producing a train of 40 kA pulses of 3 ps duration as the drive beam for CLIC using an rf linac driven free electron laser (FEL) buncher. Potential debunching effects are discussed. Finally we describe a low energy test experiment.

1. Introduction

Among the many technoligical challenges of the CLIC two-beam accelerator scheme [1] to realize a TeV linear collider of electrons and positrons one of the most difficult is the generation of the driven beam. In one scenario, the CLIC driven beam would be composed of 40 kA bunchlets of = 3 ps duration (σ_0) with a total charge of = 160 nC. Eleven bunchlets are repeated at a frequency of 30 GHz to form a pulse train that is repeated four times at a frequency of 352 MHz to form a macropulse. The macropulses must be generated at a repetition rate of = 1.5 kHz. These features are summarized in table 1.

Clearly the most difficult feature of producing the driven beam is the formation of such high charge, picosecond duration bunchlets at energies < 50 MeV. As it is unlikely that the bunchlets can be generated directly from a cathode with the desired waveform, one must consider other strategies, all of which involve one or more stages of bunch compression.

The consequences of the bunching properties of a high gain FEL have been investigated theoretically [2J and demonstrated experimentally [3], but the bunching of the beam current per se has never been measured. Recently Shay et al. [4] have proposed the use of a high gain FEL operated beyond saturation, driven by a 15 MeV, 2-3 kA linear induction accelerator to generate the CLIC drive beam. Here we extend to higher currents the ELFA high gain FEL [5] with wave guide slippage control driven by a 10 MeV superconducting rf linac operating at 352 MHz. In particular we propose to furnish the drive beam for CLIC with an amalgam of magnetic switching, rf-accelerator and FEL technologies. The use of a radio frequency linac facilitates the control of energy spread in the beam and makes it more practical to extend beam energy up to 40 MeV if desirable. The use of a low frequency rf-accelerator avoids several technological difficulties related to voltage regulation in induction linacs [4,6]. Moreover, the 352 MHz linac is easily phâsed locked to the main drive beam linac.

At the entrance to the 30 GHz FEL buncher which compresses the beam current into 40 kA, 3 ps bunchlets, we require a beam of = 4 kA at = 20-30 MeV. The beam train begins with a high voltage, high current electron gun. One such gun with suitable characteristics is the SHOGUN [6,7] presently under construction by Science Research Laboratory to be tested at UCLA. SHOGUN consists of a small thermionic cathode generating a 400 A, 1.5 ns beam in a 1.25 MeV induction stack driven with SNOMAD magnetic pulse compressors. Beam extraction is controlled with a grid driven by ferrimagnetic shock lines. At the exit of the electron gun, rf bunching cavities or an FEL pre-buncher can be used to compress the beam to a 4 kA, 120 ps pulse prior to its acceleration to 20-30 MeV in cryogenically cooled, high field 352 MHz cavities. The 20 MeV beam is injected with a 30 GHz signal into a waveguide

Table 1
Features of the CLIC drive beam

Peak bunchlet current, I_{peak}	40 kA
Bunchlet rms duration	3 ps
Charge per bunchlet, Q	160 nC
Bunchlet spacing	1 cm
Bunchlet frequency	30 GHz
Bunchlets per pulse	11
Pulse frequency	352 MHz
Pulses per macropulse	4
Macropulse frequency	1500 Hz

inside a short, high field wiggler. Operating with beam high currents, the FEL process leads to high gain of the 30 GHz signal and rapid bunching of the beam. The termination of the FEL well before saturation maximizes the compression of the beam current and minimizes the energy spread to yield the peak currents and waveform desired from CLIC. As the initial 1.5 ns pulse can only yield three bunchlets the entire pulse train is produced by four lines running in parallel. The subsequent rapid acceleration prevents space charge debunching. A schematic of this scheme using a FEL pre-buncher is shown in fig. 1.

2. The high gain FEL as a buncher

When a beam traverses the FEL wiggler of period, A_w, radiation is generated at the resonant wavelength λ_s. As the signal grows the pondermotive potential created by the wiggler field and the radiation bunches the beam electrons periodically on the wavelength scale of the resonant (sometimes called optical) wavelength. The current compression due to the FEL action can be computed from the bunching parameter, b, which is the ensemble average

$$b = |\langle e^{-i\theta} \rangle|,$$

where 0, is the phase of the ith electron with respect to the radiation field. For an unbunched beam, $b = 0$ while for a beam bunched to a delta function of current, $b = 1$. The strong FEL bunching is

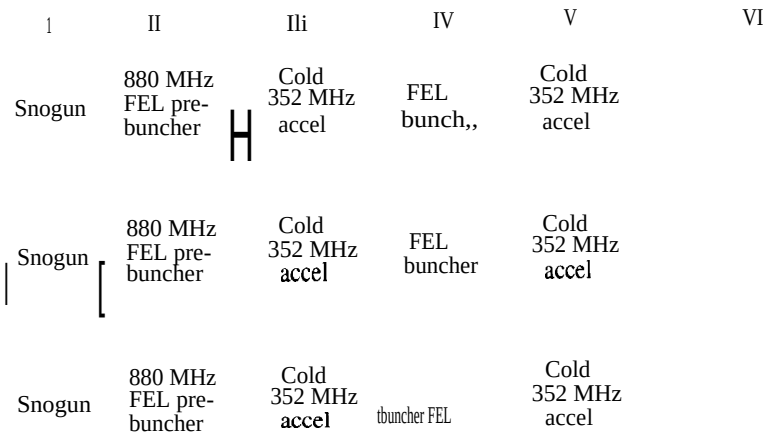

Fig. 1. The proposed generator chain for the CLIC drive beam: Section *I-1.25* MeV; *1.2* ns; *500 A;* Section *II-1.25* MeV; 1 bunch *120 ps; 5 kA;* Section *111-25* MeV; 1 bunch @ *120 ps; 5 kA;* Section *IV-25* MeV; *4* bunches @ *3 ps; 50* kA; *30 ps* spacing; Section *V-50* MeV; *4* bunches @ *3 ps; 50* kA; *30 ps* spacing; Section *VI-3* GeV; *12* bunches 4 *3 ps; 50* kA.

evidenced from the fact that when the gain saturates the bunching factor reaches a maximum $b_{max} = 0.8$ regardless of the actual values of the initial current, λ_w, or A_s.

The gain of the FEL and the speed of the bunching process is described by the BPN universal scaling parameter [2], p;

$$p \equiv \frac{1}{\gamma}\left(\frac{a_w \omega_p}{4ck_w}\right)^{1/3} \propto \frac{J^{1/3} B_w^{2/3} \lambda_w^{4/3}}{\gamma}$$

where y is the usual relativistic factor, ω_p is the non-relativistic plasma frequency, a_w is the dimensionless vector potential of the wiggler, k_w is the wiggler spatial frequency, B_w is the wiggler peak field and J is the beam current density.

$$a_w = 0.66 B_w[\text{Tesla}]\lambda_{w\,[\text{cm}]}$$

We note the experimentally verified feature of the high gain FEL, namely that the rate of the bunching action is proportional to $p \propto I_b$; hence the bunching actually proceeds more rapidly as the input current increases. In fact, in the experiment of ref. [3] the bunched current inferred from the well-verified simulations of the experiment was = 10 kA (though this feature was never measured). It is this characteristic that makes the FEL buncher so attractive in comparison with other bunching schemes when the final peak value of the bunched current must be extremely large as in the case of the CLIC drive bunches. If the initial current pulse is several optical wavelengths long, the output current from the FEL will be a train of high current bunchlets spaced at the optical wavelength. With respect to the requirements of the CLIC drive beam, achieving a precisely controlled bunchlet spacing at the desired interval corresponding to 30 GHz is a natural consequence of FEL action.

Another feature of the FEL that compares favorably with respect to other bunching schemes is that the length over which bunching occurs scales favorably (increases linearly with increased beam energy). The FEL action does, however, induce an energy spread in the beam that is proportional to the gain. By terminating the wiggler before the FEL process saturates one can a) maximizes current multiplication, b) keep the induced energy variation small, and c) minimizes wiggler length, allow the correlated energy variation to continue to bunch the beam in the transport beyond the wiggler. This last effect is just the bunching action of a high gain optical klystron which has been described analitically without space charge in ref. [8].

3. Potential limiting phenomena

We now turn our attention to phenomena that can limit the performance of the FEL bunching process:

a) energy spread at the entrance to the wiggler,
b) loss of the radiation field via diffraction,
c) transverse and longitudinal space charge debunching.

3.1. *Effects of energy* spread

With respect to the intrinsic energy spread that is produced by the acceleration process upstream of the buncher the FEL compares well with other techniques. Quantitatively, we expect the FEL to be insensitive to instantaneous energy spreads and variations as long as

$$\frac{\Delta\gamma}{\gamma} \gtrsim \text{accelerator } C^{P}.$$

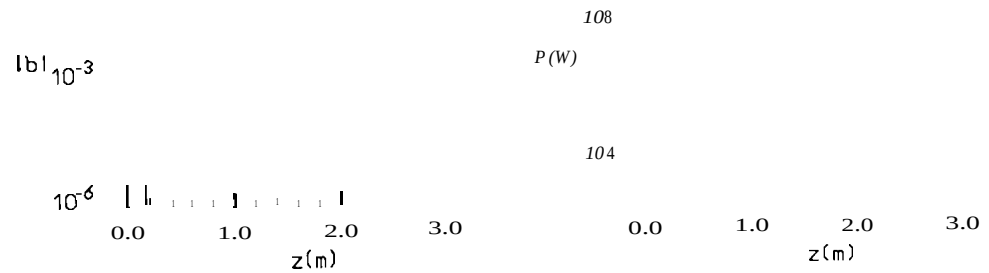

Fig. 2. GINGER Simulation of the FEL parameters in table 2. We show (a) the bunching parameter *b* and (b) the output power in Watts, in a logaritmic scale, as a function of the length of the wiggler, Z(m). For an explanation of the marked points refer to fig. 3.

As the FEL (or rf-cavity) pre-buncher in fig. 1 is followed by an accelerator section that increases the mean beam energy by a factor of = 5, this requirement is easily satisfied especially as the wiggler is actually truncated before saturation is reached. Moreover, even the strong super-radiant regime can be used in our scheme. In this case the sensitivity of the FEL is further reduced with respect to both the instantaneous energy spread or to the energy variation in the beam.

3.2. Loss of the radiation field via diffraction

In optical FELs using very low emittance beams the gain can be reduced and the bunching speed decreased if the radiation diffracts out of the electron beam too rapidly. In our case this consideration does not apply as the radiation is confined to the region close to the beam by the waveguide that we use to control the slippage of the radiation field with respect to the electron beam. The effectiveness of the waveguide in eliminating the degradation of performance due to diffraction is displayed by the results of a full three dimensional simulation with the code GINGER [9] that includes the effects of longitudinal space charge forces.

In figs. 2 and 3 we show the GINGER simulations with the output power and bunching as a function of the length of the wiggler (fig. 2) and also the histogram of the current and the electron longitudinal phase-space in a wavelength (fig. 3). Note in fig. 2 the link between the FEL gain and the bunching mechanism and the strong bunching action that derives from the combination of the dispersive path in the wiggler and the strong ponderomotive potential.

Thus we are left with charge as the only potentially deleterious effect.

Table 2
Parameters of the GINGER runs

Peak bunchlet current, (peak	4 kA
Radiation wavelength, A_s	1 cm
Beam energy	9.5 MeV
Wiggler wavelength, λ_w	24 cm
Wiggler field, B_w	2.5 kG
FEL parameter, p	0.13
Waveguide heigth, *b*	2.5 cm
Normalized beam emittance, ϵ_n	0.1 π cm rad
Input power, P_0	1 kW
Output power, ρP_{beam}	$\simeq$ 5 GW
Saturation length Z_{sat}	3.5 m

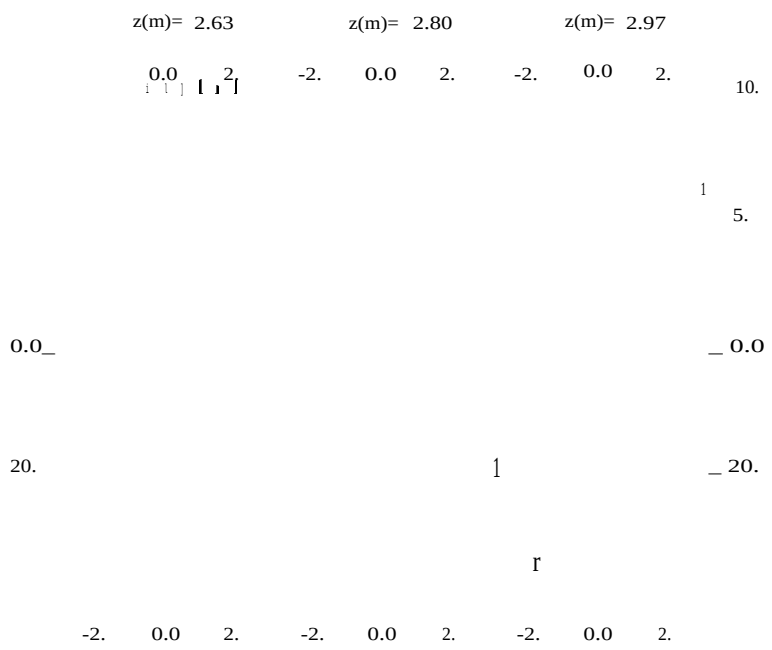

Fig. 3. Phase histogram, showing the electron current in a wavelength (top). Electron distribution in the longitudinal phase space (bottom). I_0 is the average input electron current. Note the strong peak current that can be obtained if one stops the wiggler at the proper point (Z = 2.84 m). The outputs shown here are at the points marked in fig. 2.

3.3. Transverse space charge effects

To begin our analysis we consider first the problem of the transverse space charge. Outside the bunched beam of radius R the radial electrostatic field, E_r, is

$$E_{r,\mathrm{peak}}(r) = -\frac{\underline{\mathrm{peak}}}{2\epsilon_0\pi c\beta r} \quad \frac{60 I_{\mathrm{peak}}[\mathrm{A}]}{r[\mathrm{m}]}\ [\mathrm{MV/m}].$$

In eq. (6) c is the speed of light, c_0 is the permittivity of free space, and ß is the velocity of the electrons, v, divided by c. For the 40 kA CLIC bunchlet at 20 MeV with an rms radius of 3 mm the radial electric field evaluated at the edge of the beam is = 800 MeV/m. Thus transverse space charge would

Table 3
Parameters of the FEL test

Peak bunchlet current, I_{Peak}	10A
Radiation wavelength, A,	1 cm
Beam energy	2.5 MeV
Wiggler wavelength, λ_w	12 cm
Wiggler field, B_w	1.8 kG
FEL parameter, p	0.018
Waveguide heigth, b	1.7 cm
Normalized beam emittance, ϵ_n	0.1 π cm rad
Input power, P_0	1 kW
Output power, P_{beam}	= 0.5 MW
Saturation length Z_{sat}	=5m

be disastrous were it not for the fact that a relativistic beam carries its own extremely strong, azimuthat focussing field, B_θ,

$$B_\theta(r) = \frac{\mu_0 I_{peak}}{2\pi r} = \frac{I_{peak}[A]}{r[cm]} \text{ [gauss].}$$

Once we include this pinch field in the Lorentz force equation we find that the relativistic electrons experience very little radial force,

$$F_r = e(E_r - vB_\theta). \quad (9)$$

Noting from eqs. (6) and (7) that

$$B_\theta = \frac{v}{c} E_r,$$

we obtain the well known result

$$F_r = eE_r\left(1 - \frac{v^2}{c^2}\right) = \frac{1}{\gamma^2} eE_r. \quad (10)$$

Recalling that 1 gauss = 3×10^4 V/m, we can see that outside of the wiggler at 20 MeV even a 40 kA bunchlet can be confined radially against space charge expansion by a magnetic field equivalent to a B_θ of only a few tens of gauss. In fact, a larger field is actually needed to prevent the beam from expanding due to its finite emittance.

The relative effects of the emittance, E, and transverse space charge on the beam as it propagates in the z direction can be evaluated both outside of and within the wiggler through the use of the envelope equation for the rms radius of the beam,

$$\frac{d^2R}{dz^2} = \frac{E^2}{R^3} + \frac{U}{R} + \frac{\langle K_\beta^2 R^2 \rangle}{R} = 0.$$

The transverse self-fields of the beam are described by potential U and the external focussing by the term K_β. If the external focussing can be described by an harmonic potential with betatron frequency k_β, the ensemble average in the last term is reduced to the simple product k.R. In the wiggler the betatron frequency is

$$k_\beta = \frac{2\pi}{\sqrt{2}\lambda_w\gamma} = \frac{2\pi a_w}{\sqrt{2}\lambda_w\gamma} \quad (12)$$

In the absence of space charge neutralization from a background plasma the potential U may be expressed in terms of the Alfv6n current as

$$U = -\frac{I[kA]}{17[kA]\gamma^3}. \quad (13)$$

The envelope equation implies a unique equilibrium radius for the beam, R_e,

$$R_e = R_0(f + V1 + f^2)^{1/2} \quad (14)$$

where $R_0 = \frac{E_{Ik}}{} = 6 \times 10^{-2} \sqrt{\epsilon[mrad]/B(I)}$ is the equilibrium radius in the absence of space charge and

$$f = \frac{U}{2\epsilon K_\beta} = \frac{U_\gamma}{2\epsilon_n K_\beta} = \frac{10^{-4} I[kA]}{B_w[T]\epsilon_n\gamma} \quad (15)$$

In eq. (15) we have introduced the normalized emittance, E_n, which is equal to ye. From eqs. (14) and (15) we can see that the transverse space charge effects can be ignored when

$$E° \quad \frac{U\gamma}{2k_{\beta}} \quad \frac{10^{-4}I[\mathrm{kA}]}{{}_{y}B_{W}[T]} \tag{16}$$

To satisfy the high gain FEL conditions, the phase area of the electron beam should be smaller than that of the radiation; i.e.,

$$E_n < \frac{\lambda_s \gamma}{2\pi}. \tag{17}$$

For a 40 kA bunchlet at 20 MeV, $B_W = 0.66T$ both eqs. (16) and (17) will be satisfied when

$$1.5 \times 10^{-4} \text{ mrad} < E_n < 6.2 \times 10^{-2} \text{ mrad}. \tag{18}$$

This condition is easily satisfied for our proposed injector for the CLIC drive beam; we can choose a value $E_n = 2 \times 10^{-3}$ m rad so that the beam has a convenient radius (= 3 mm) with respect to the height of the waveguide. From this discussion we conclude that the neglect of transverse space charge effects in the GINGER simulation upon which we would base a final design is justified.

3.4. Longitudinal space charge debunching

The longitudinal space charge forces depend on the geometry and distribution of charge in the bunch and on the external boundary conditions. With respect to the FEL action in the wiggler, these dependences are already included in the GINGER code. Therefore, we need to focus our attention on the debunching at the output of the wiggler.

Supposing that the beam pipe is much bigger than any dimension of the beam, we will ignore its presence. If the beam pipe is considered, as quoted in ref. [4], the beam pipe shape can be modeled to present an inductive impedance, which in turn decreases the field within the bunch and consequently the space charge effects.

In a round, perfectly conducting beam pipe, for a bunch such that $b \ll \gamma\sigma_{z,\mathrm{lab}}$, the field on axis can be written:

$$E_z(z, r=O) = -\frac{R2}{2\epsilon_0\gamma^2}\left(\frac{1}{2} + \ln\frac{b}{R}\right)\frac{\mathrm{d}n_e}{dz}, \tag{19}$$

where b is the beam pipe radius, R the beam radius, n_e is the longitudinal charge distribution and o,,,,,, is its characteristic length in the lab frame (see appendix).

Let's now consider the free space case. We will suppose a Gaussian longitudinal density profile and a square radial profile. In a frame solidal with the bunch:

$$p(r, z) = \frac{Q_0}{\pi R^2 \; 2\text{-}rr\, o_L} \exp\left(-\frac{z}{20}\right). \tag{20}$$

The field on-axis can be calculated from:

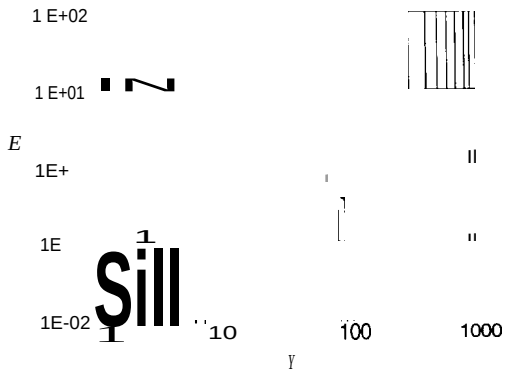

Fig. 4. Peak electric field on axis (MV/m) as a function of the beam Lorentz factor, y. The solid line corresponds to a numerical integration of expression (21), the dashed line shows the analytical expression (24). Here σ_z =1 mm and R = 3 mm.

Splitting the integral and integrating two times by parts, we obtain (now everything in the lab frame):

$$E_z(r=0,\ z=z_0) = \frac{Q_0}{(2\pi)^{3/2}\epsilon_0\gamma^2\sigma_z^2}\left[e^{-z_0^2/2\sigma_z^2}\log\left(\frac{R}{\ }\right) + \frac{\gamma R}{2}\int_0^{\infty}\left[\left[1-\left(\frac{z_0}{\sigma_z}+t\right)^2 e^{(z_0/\sigma_z+t)^2} - 1 - \left(\frac{z_0}{\sigma_z}-t\right)^2 e^{(z_0/\sigma_z-t)^2/2}\right.\right.\right.$$
$$\left.\left.\left. \times\left(2 - \frac{1}{2}\left(t\sqrt{t^2+\frac{R^2}{\gamma^2\sigma_z^2}} + \frac{R^2}{\gamma^2\sigma_z^2}\log\left(t+\sqrt{t^2+\frac{R^2}{\gamma^2\sigma_z^2}}\right)\right)\right)\right]\right] dt \quad (22)$$

It can be shown (numerically) that the integral on the right hand side of this equation becomes roughly independent of $R/\gamma\sigma_z$ for $R/\gamma\sigma_z < 0.1$ (see fig. 4). As a function of z_0/σ, moreover, it is to a good approximation, linear within 0 and 1. So, for $R/\gamma\sigma_z < 0.1$ and $0 < z_0/\sigma < 1$, we can write

$$E_z(r=0,\ z=z_0) = \frac{Q_0}{(2\pi)^{3/2}\epsilon_0\gamma^2\sigma_z^2}\left[\sigma_z e^{-z_0^2/2\sigma_z^2}\log\left(\frac{\gamma\sigma_z}{R}\right) + 0.265\frac{z_0}{\sigma_z}\right]. \quad (23)$$

In particular for $z_0 = \sigma_z$, where the field is about maximum:

$$E_z(r=0,\ z=\sigma_z) = \frac{Q_0}{(2\pi)^{3/2}\epsilon_0\gamma^2\sigma_z^2}\left[e^{-1/2}\log\left(\frac{\gamma\sigma_z}{R}\right) + 0.436\right]. \quad (24)$$

For Q_0 = 160 nC, σ_z = 1 mm, y = 40, R = 3 mm, this yields:

$$E_z(r=0,\ z=\sigma_z) = 1.32\ [\mathrm{MV/m}]. \quad (25)$$

Now we can evaluate the space charge induced energy spread, Ay/y, and the "debunching", $\Delta L_b/L_b$, for a "travelled distance". We will evaluate these fractional variations to 0-order for a drift of 1 m. If we assume that the particle at σ_z always experiences the same field during the flight time (no debunching) and that there is no initial energy spread,

$$\frac{\mathrm{Ay}}{\gamma} \simeq \frac{eE_z L}{\gamma mc^2} \simeq 2E_z[\mathrm{MV/m}]L[\mathrm{m}] \quad (26)$$

With the previous parameters, between the particle at Q_z and the particle at the center of the bunch, after 1 m,

$$\frac{\Delta\gamma}{\gamma}_{y} = \frac{2.64}{40} = 6.6\%. \tag{27}$$

If we assume that $\Delta\gamma/\gamma$ grows linearly during the flight time, we can write

$$\frac{\Delta L_b}{L_b} \frac{1}{2}\gamma^2 - 1 \frac{\Delta\gamma}{\gamma} \tag{2g}$$

where L_f indicates the drift length and where $L_b = \sigma_z$. With the previous parameters

$$\frac{\Delta L_b}{L_b}$$

Note that for R/yo-_ small enough, as Ay is proportional to Eℓ and Eℓ (apart from a log(y) term) goes like y^{-2}, $\Delta L_b/L_b$ goes like y^{-5}! These two fractional variations have been calculated numerically dividing the bunch (between -5Q_z and 5o-,) in 500 slices, each considered as a uniform cylinder, and integrating the fields and the particle motion during the flight time. This calculation yeld

(30)

y

If we require the bunch energy spread and the debunching to be little, say both are < 0.1, we can evaluate the maximum drift allowed before these limits are exceeded

$$\frac{\Delta\gamma}{\gamma}_{y} = \frac{2E_z[\mathrm{MV/m}]L_f[\mathrm{m}]}{y} < 0.05 \tag{32}$$

implies

$$L_f < \frac{0.05y}{2E_z} = 76\ [\mathrm{cm}] \tag{33}$$

Note that we wrote 0.05 on the right hand side of eq. (32). This is because, up to this point, by $\Delta\gamma/\gamma$ we meant the fractional variation between the particle at or and the center of the bunch. The debunching condition yelds

$$0.1\sigma_z(\gamma^2 = \underline{1)y}$$

z

If both eqs. (33) and (34) are to be satisfied the maximum allowed drift will be the minimum of the two.

If these distances seem somewhat shorter than practical, one can increase the energy of the beam. An increase to 40 MeV would abolish space charge effects for all practical purposes. These features have been already confirmed by preliminary calculation performed with PARMELA for a beam expanding inside a solenoidal B field in otherwise free space. The PARMELA simulations assume the beam to have a uniform hard edge electron beam distribution, which certainly increases space charge effects at the beam boundary. Nevertherless for a 20 MeV we find a debunching length of 3 m and at 40 MeV more than 30 m. More detailed simulations including the effects of the Gaussian distribution of charge and of the beam pipe boundary conditions will be presented elsewhere.

The FEL has a second, unique feature that helps to defeat space charge debunching. We have shown that the correlated natures of both the FEL-induced energy variation in a bunch and the space-charge

Fig. 5. A illustration of the actions of the FEL and space charge forces on the longitudinal phase space of the beam. The origins of the energy and phase coordinates are taken to be the mean energy and the central reference. (a) The phase space distribution in the wiggler prior to saturation. The tendency (shown by the arrows) is for the beam to bunch via the usual klystron mechanism. (b) Space charge forces tend to increase the energy of the front half of the beam and lower the energy of the trailing half. (c) The combined tendencies of the klystron action and the space charge forces.

induced energy variation are such that their combined action in the drift section downstream of the wiggler not only continues (for a certain amount of time) the bunching action, but actually acts to reduce the total energy spread. This prcess is illustrated in fig. 5. panel (a) illustrates the longitudinal phase space of the beam in the wigg r at a point prior to saturation of the FEL process. As the beam propagates in the transport, its tendency (shown by the arrows) is to continue to bunch the beam via the usual klystron mechanism. The space charge forces tend to increase the energy of the particles in the front half of the beam and lower the energy of the trailing half, leading to the tendency of the longitudinal phase space distribution to deform in the manner indicated in (b). The combined tendencies of the klystron action and of the deformation due to space charge forces is to reduce the energy spread as the pulse continues to bunch as indicated in (c). The quantitative features of these combined processes are sensitive to the exact point of stopping the FEL action. An optimization study is now in progress and will be described elsewhere. We emphasize, however, that to take advantage of this continued bunching action it is essential that one stop the FEL process prior to saturation unlike in the bunching scheme proposed by Shay et al.

Finally we point out that the extension of FEL energy from 20 to 40 MeV with an rf-linac does not present any serious problem because the FEL scaling laws are such that the increase in y can be compensated by increasing the wiggler period. This will be discussed in detail elsewhere. In addition, the longer wiggler period makes the construction of the wiggler easier.

4. Suggested test experiment at 10 A and 2.5 MeV energy beam

All the bunching properties of the rf-linac driven FEL with waveguide control of slippage can be tested in a low energy, low current experiment. Novel features of this experiment include the measure-

ment of the bunched current, slippage control in the FEL, and strong super-radiant behavior of the FEL. With the same wiggler as we would use with the full 20 MeV, 4 kA beam, the laser gain will be nearly the same as the gain scales as $p = I'^{/3}$. If we decrease I by a factor 400 from 4 kA to 10 A, we should simultaneously decrease the beam energy y by a factor of 6.6, down to 2.5 MeV. Then the saturation length of the FEL amplifier will remain unchanged. Furthermore the low energy experiment allows us to test all the relevant properties of space charge debunching. Imposing that $(\Delta\gamma/\gamma)_{sc}$ is much longer than the intrinsic FEL linewidth p, i.e., (Ay/y)s, > p and using the previous expression we have

$$L[m] >> \frac{\gamma^3\sigma_0^2\rho 10^5}{2\lambda I} = 10^2\rho \tag{35}$$

For the suggested parameters for the experiment: y = 6, 1= 10 A, $o-_0 = 1$ mm, A = 1 cm, the FEL parameter, $p = 2 \times 10^{-2}$; hence, for distances L exceeding 1 m space charge effects will dominate the debunching process and will be readily distinguishable from debunching due to the FEL induced energy broadening.

5. Conclusions

We have shown that the rf-FEL buncher appears to be a promising scheme to provide the CLIC drive beam. Issues related to space charge can be made negligible by the appropriate choice of energy at the input to the wiggler. Finally we have described the characteristics of a low current, low energy test experiment that would demonstrate all the relevant physics of our proposed scheme.

Acknowledgements

One of us (WAB) would like to thank the Milano Section of INFN for its kind hospitality during the preparation of the report. This work is partially supported by Lawrence Livermore National Laboratory under US Dept. of Energy contract W-7405-ENG-48.

References

[1] W. Schnell, CERN LEP-RF-88-59, June, 1988.
[2] R. Bonifacio, C. Pellegrini and L. Narducci, Opt. Commun. 50 (1984) 373.
[3] T.J. Orzechowski et al., Phys. Rev. Lett. 54 (1985) 889.
[4] H.D. Shay, R.A. Jong, R.D. Ryne, E.T. Scharlemann, S.S. Yu and E.T. Scharlemann, Proc. 12th Int. FEL Conf., Paris, 1990, eds. J.M. Buzzi, J.M. Ortega, Nucl, Instr. and Meth. A304 (1990) 262.
[5] R. Bonifacio et al., Proc. European Particle Accelerator Conference, Nice, June, 1990.
[6] W.A. Barletta, European Particle Accelerator Conference, Nice, June, 1990.
[7] W.A. Barletta and S. Hartmann, UCLA report, UCLA-CAA00070-1-91, January, 1991.
[8] R. Bonifacio, R. Corsini and P. Pierini, Phys. Rev. A45 (1992) 4091.
[9] W. Fawley and T. Scharlemann, Lawrence Livermore National Laboratory.
[10] R.J. Briggs and V.K. Neil, Plasma Phys. 8 (1966) 255.
[11] M. Abramowitz end I. Stegun, Handbook of Mathematical Functions (Dover, New York).
[12] H.D. Shay et al., Nucl. Instr. and Meth. A304 (1991) 262.

Appendix A. Solution of the Poisson equation for the space-charge field

Let us consider the equation for the electrostatic space charge field in the moving frame of the electrons:

$$\nabla^2 E = -\frac{1}{E0}\nabla\rho. \tag{36}$$

Assuming a density function of the form $p = \epsilon_0 n_e(z)\chi(r)$, where n_e is the longitudinal electron density and $X(r)$ the radial profile of the beam, assumed here, for sake of simplicity, to be a step function of width R (the beam radius).

Fourier transforming along z the longitudinal component of eq. (36), we obtain the following differential equation for the Fourier component of the space charge field, $\tilde{E}_z(k, r)$:

$$r^2 \frac{\partial^2 \tilde{E}_z}{\partial r^2} + r \frac{\partial \tilde{E}_z}{\partial r} - k^2 r^2 \tilde{E}_z = -ikr^2 \tilde{n}_e(k)\chi(r), \tag{37}$$

where "e(k) is the Fourier tranform of the longitudinal charge density.

From the Maxwell equation $\nabla \times E = 0$, we can derive the following relation between the Fourier transforms of the longitudinal and radial field:

$$ik\tilde{E}_r(k, r) = \frac{\partial \tilde{E}_z}{\partial r}(k, r), \tag{38}$$

hence, differentiating the solution of eq. (37) with respect to r we can find the expression for the Fourier transform of the transverse space charge field.

The solutions of the homogeneous differential equation associated with the expression (37) are the modified Bessel functions 1_0 and K_0. We can easily solve this differential equation studying the solutions for $r < R$ and $r > R$ and imposing the continuity of the fields for $r = R$. A similar technique, along with the specification of the boundary conditions of the problems, allows us to write explicitely the exact form of the Fourier components of the fields.

We now investigate two cases with different boundary conditions: the beam pipe case and the free-space case.

Appendix B. Beam pipe case

In order to find a solution for eqs. (37) and (38) in a beampipe of radius b, we must require the proper boundary condition, that is $E_z(z, b) = 0$. This condition transforms to $\tilde{E}_z(k, b) = 0$ and leads to the following expression for the transformed field inside the beam $(r < R)$:

$$\tilde{E}_z(k, r) = -ik\tilde{n}_e(k)\left\{\frac{R}{|k|}\left[\frac{K_1(|k|R)}{I_1(|k|R)} + \frac{K_0(|k|b)}{I_0(|k|b)}\right] I_1(|k|R) I_0(|k|r) - \frac{1}{|k|^2}\right\}$$

Eq. (39) is the expression of the transformed longitudinal field, which upon inverting the fourier transform, would give the exact space charge field as a function of r and z.

B.1. Limit case: b << oz

We now evaluate the on-axis $(r = 0)$ field in the case $b \ll \sigma_z$ (or $b \ll y\sigma_z$ in the lab-frame), where a_z is the beam characteristic length.

In the limit where the function $\tilde{n}_e(k)$ has a narrow band, of width u_k, such that $\sigma_k b \ll 1$, the Bessel function can be expanded for small arguments, giving the following result

$$\tilde{E}_z(k, r = 0) = -(-ik\tilde{n}_e(k))R^2\left(\frac{1}{2} + \ln\frac{R}{b}\right). \tag{40}$$

By the fourier transform properties the first term in the brackets is the transform of the derivative with respect to z of the function $n_e(z)$, hence, transforming back in the real space:

$$E_z(z, r = 0) = -\frac{R^2}{2\epsilon_0}\left(\frac{1}{2} + \ln\frac{b}{R}\right)\frac{dn_e}{dz}. \tag{41}$$

The limit $\sigma_k b << 1$ can be transformed, in real space, in the limit $\sigma_b >> b$, since $\sigma_k \sigma_b \approx 1$, by Fourier transform properties. We note that an expression similar to eq. *(41)* can be found elsewhere and can be derived applying the circuitation theorem in the beam pipe [12].

Appendix C. Free space case

In the case of free space propagation, we must require require a bounded solution for E_z as r - -, and the continuity of the longitudinal transverse fields for r = R. These requirements determine the following structure for the transform of the longitudinal electric field inside the beam

$$\tilde{E}_z(k, r) = -(ik\tilde{n}_e(k))\left[\frac{}{|k|}K_1(|k|R)I_0(|k|r) - \right. \quad \text{lclzJ.} \tag{42}$$

C 1. Limit case. R << σ_z

In the case of $R << \sigma_z$ *(R << yoσ_z* in the lab-frame), hence $u_k R << 1$, we can expand the Bessel functions and derive the following expression for the on-axis transform of the longitudinal field:

$$\tilde{E}_z(k, r=0) = \frac{ik\tilde{n}_e(k)}{2}\left[R^{l} \quad \text{In} \quad \frac{|k|R}{2} \right. \quad 1. \tag{43}$$

Hence, in this case the longitudinal electric field is given by the following expression:

$$E_z(z, r=O) \_ \quad \frac{z}{o} \quad \pi \int \quad dk\left(-ik\tilde{n}_e(k)\right) \text{In I} \quad \frac{21R}{} \quad e^{-ikz}. \tag{44}$$

Although it does not seem possible to evaluate this integral, we can split it in two contributes, as follows:

$$E,(z, 0) = \frac{R^2_0}{2e_0} \quad 1 \quad \int_{-\infty}^{\infty} dk\left(-ik\tilde{n}_e(k)\right)\left[\ln \frac{R}{} + \text{In} \quad \frac{\sigma_z |k|}{2} \quad 1 \right. \quad e \quad z$$

or, integrating the fist term explicitely

$$E,(z, 0) \_ \frac{Rz}{2\epsilon_0}\ln \quad \frac{R}{\nu_z} \frac{dn_e}{dz} + \frac{R^z}{2e_0} \quad 1 \quad -\pi \quad dk\left(-ik\tilde{n}_e(k)\right)\ln \quad \frac{\sigma_z |k|}{2} \quad e^{-ikz}. \tag{45}$$

noting that the first term of this expression, considering the case of Gaussian distributions for $n_e(z)$, and for z = o-$_z$, corresponds exactly to the first term of expression (24).